

Silicon-Processed Microneedles

Liwei Lin and Albert P. Pisano

Abstract—A combination of surface- and bulk-micromachining techniques is used to demonstrate the feasibility of fabricating microhypodermic needles. These microneedles, which may be built with on-board fluid pumps, have potential applications in the chemical and biomedical fields for localized chemical analysis, programmable drug-delivery systems, and very small, precise sampling of fluids. The microneedles are fabricated in 1, 3, and 6 mm lengths with fully enclosed channels formed of silicon nitride. The channels are 9 μm in height and have one of two widths, 30 or 50 μm . Access to the channels is provided at their shank and distal ends through 40- μm square apertures in the overlying silicon nitride layer. The microneedles are found to be intact and undamaged following repetitive insertion into and removal from animal-muscle tissue (porterhouse steak). [379]

Index Terms—Drug-delivery, fluid sampling, microchannel, microneedle.

I. INTRODUCTION

RELIABLE microhypodermic needles can be expected to have broad applications to fluid sampling, fluid delivery, and precisely located chemical-reaction stimulation. If they are robust enough to penetrate biological tissue, applications to biomedical and neural measurements, drug-delivery systems, and microbiological sample analysis are expected [1]–[3].

Recent research has successfully demonstrated electrical microprobes made of silicon for an IC-compatible, multichannel neural-recording array [4]. These silicon microprobes with cross sections on the order of tens of micrometers can penetrate living tissue without causing significant trauma. In order to better understand the behavior of biological neural networks with respect to chemicals (drugs), it is important to be able to deliver liquids in precise quantities while monitoring the neuronal responses in vivo [1], [2]. It is expected that the capability of combining fluid-delivery channel with neural-recording array will have broad applications.

Microneedles that are fabricated from IC-compatible processes have a distinct advantage owing to the feasibility of on-chip electronics which can form a part of a chemical design-and-analysis system or can provide drive electronics for pumps and valves [5]. The silicon-processed microneedles described here have been fabricated with fully enclosed channels for the transport of liquids or gases. The channels can run the length

of the needle (making possible chemical sampling or delivery), and they can also be formed into networks at the shank end of the needle.

The facility for bubble-powered micropumps is integrated into the microneedles in the form of a series of polycrystalline silicon heater strips running across the floor of the channels at the shank end. Prior research has shown that microbubbles, capable of actuating a polycrystalline silicon cantilever [6], could be formed in fluids using similar resistors heated by 5-V, 11-mA pulses [7]–[9]. Other micropumps can also be employed with these microneedles, such as those actuated by ultrasonic Lamb waves [10], piezoelectrics [11]–[13], and electrohydrodynamics [14], [15].

II. DESIGN OF MICRONEEDLES

A sketch of a silicon-processed microneedle is shown in Fig. 1. The cross section A-A of the microneedle shows the interior of the fully enclosed flow channel that runs along its length. The micro hypodermic channels are surface-micromachined onto a silicon substrate that is mostly etched away in the final fabrication step. A thinned (about 50 μm) layer from the original substrate is retained by using a timed etch process. Near the tip of the needle, features of corner etching by the anisotropic etchant reduce the thickness to about 12 μm of heavily boron-doped silicon. The retained single-crystal silicon provides a rigid spine to add strength to the microneedle. At the shank end, the substrate material widens out to a 50- μm thickness and a large surface area, suitable for the incorporation of integrated electronic and/or fluidic devices. A similar design feature without the flow channel has been previously described [4].

The flow channel runs the length of the microneedle (from 1–6 mm) and has openings near the distal and shank ends. Near the shank end is a series of thin polysilicon resistors that cross the floor of the flow channel. These are intended to form a thermally driven, cascaded-bubble micropump.

In order to form the enclosed channel, it is necessary to remove a sacrificial layer of phosphorus-doped glass (PSG) from within the channel region during processing. Access holes for the etch (which are filled in subsequent processing) are therefore provided at regular intervals along the channel length (each 25 μm), making the duration of the sacrificial-layer etching step independent of the channel length. The etching and silicon nitride closure procedures have been discussed earlier [16], [17].

Fig. 2(a) shows a top view of a microneedle just before it is separated from the substrate by anisotropic etching. As seen in Fig. 2(a), an “IC-interface region” of 2–3 mm² area is conveniently available. The needles have lengths of 1–6 mm

Manuscript received August 25, 1998; revised October 20, 1998. This work was supported in part by an NSF CAREER award (ECS-9734421), a grant from the DARPA/ETO/MEMS program (F30602-98-2-0227), and the Berkeley Sensor and Actuator Center, an NSF/Industry/University cooperative research center. Subject Editor, N. F. de Rooij.

L. Lin is with the Department of Mechanical Engineering and Applied Mechanics, University of Michigan, Ann Arbor, MI 48109-2125 USA (e-mail: lwlin@engin.umich.edu).

A. P. Pisano is with the Department of Mechanical Engineering, University of California at Berkeley, Berkeley, CA 94720 USA.

Publisher Item Identifier S 1057-7157(99)01447-X.

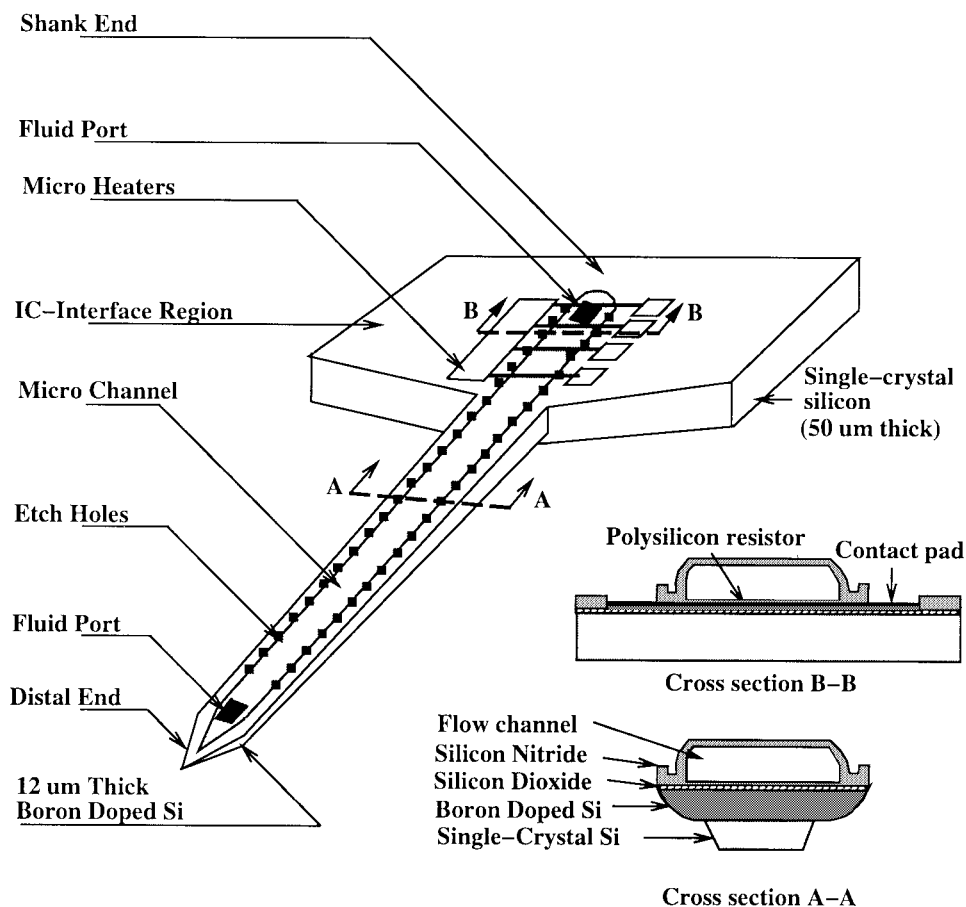


Fig. 1. Schematic diagram of a silicon processed microneedle.

and each is $80\ \mu\text{m}$ wide. The white area in Fig. 2(a) marks the separation of the needle from the original substrate using anisotropic etch [ethylenediamine pyrocatechol and water (EDP)]. Other chemical etchants or dry etching methods may be used in case these microneedles are to be used in living organisms. The dark gray area is heavily doped with boron which acts as an EDP etch stop [18]. Two heavily doped support beams connect the microneedle to the substrate and permit easy testing and manipulation of the tiny needles prior to their final use. These mechanical supports are broken easily using tweezers in order to obtain fully freed microneedles. This design permits all microneedles in a given wafer run to be attached to the substrate after the final processing step, making transport and packaging easier than if all needles were fully freed by the anisotropic etch. Moreover, no backside alignment is needed for this design in contrast to processes used for microgrippers [19] and microelectrodes [20]. The side view of the microneedle is seen in Fig. 2(b). The $50\text{-}\mu\text{m}$ -thick single crystal silicon region designed in the process is to increase the strength of the microneedle. Four-inch wafers have been used in this process such that the original thickness is about $500\text{--}550\ \mu\text{m}$.

III. MICROMACHINING PROCESSES

Fig. 3 shows cross section “A-A” (from Fig. 1) at the conclusion of key process steps. In the first step of the process, a (100)-oriented, lightly doped p-type wafer is selectively

doped with boron that diffuses at 112° for 15 h to make a $12\text{-}\mu\text{m}$ -deep heavily doped p-type region. The masking layer is thermally grown Si_2O_2 delineated by Mask 1. After this layer is removed, a 400-nm -thick layer of Si_2O_2 is thermally grown and $600\ \text{nm}$ of LPCVD low-stress nitride is deposited for passivation. A 600-nm -thick LPCVD phosphorus-doped polycrystalline silicon layer is then deposited, patterned (Mask #2), and etched. The polysilicon layer at the back side of the wafer is now etched away and a thin layer ($150\ \text{nm}$) of LPCVD low-stress nitride is deposited to cover and protect the polysilicon resistors during EDP etching. After these steps, Fig. 3(a) applies.

The wafer now goes through the microchannel fabrication sequence, which is similar to the microshell process described by Lin *et al.* [17]. First, a layer of $5\ \mu\text{m}$ PSG is deposited, followed by a layer of $3\ \mu\text{m}$ LTO (undoped LPCVD Si_2O_2). The LTO layer on top of PSG gives better adhesion to the photoresist [21] and minimizes HF attack on the interface between photoresist and PSG [22]. The microchannel is now patterned (Mask #3) and wet-etched in 5:1 BHF (buffered HF). At this point, the cross section appears as in Fig. 3(b).

Following an LPCVD deposition of $1\ \mu\text{m}$ LTO, the etch channels area is patterned (Mask #4) and wet-etched in 5:1 BHF. The wafer is then coated with $1\text{-}\mu\text{m}$ -thick LPCVD low-stress nitride and etch holes are defined (Mask #5) and etched in a plasma etcher as shown in Fig. 3(c). The sacrificial PSG and LTO inside the microchannel are etched away by

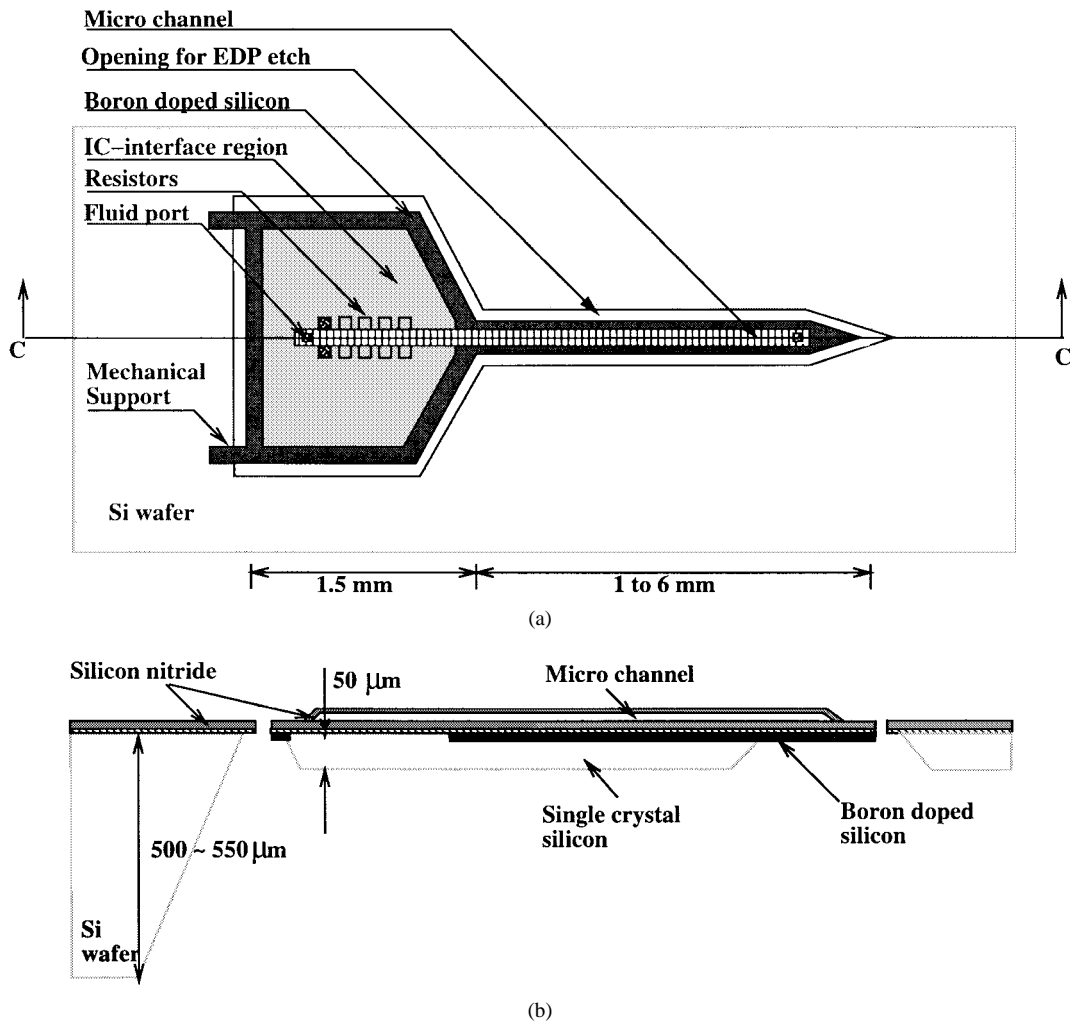


Fig. 2. Schematic (a) top and (b) side view of a silicon-processed microneedle.

concentrated HF (48% HF) and the wafer is fully rinsed in DI water. The etch-access holes are now sealed by depositing a $1.5\text{-}\mu\text{m}$ thick layer of LPCVD low-stress nitride. The final-separation EDP etch windows are now opened (Mask #6) by a plasma etcher that is stopped by design at the 400-nm -thick Si_2O_2 layer. The cross section is now as shown in Fig. 3(d).

The contact pads are now opened (Mask #7) down to the 150 nm of low-stress nitride which prevents attack at the contact sites by EDP in subsequent etching. The back side of the wafer is now patterned with a blank mask and without alignment in a stepper lithography system. This step opens up $1\text{ cm} \times 1\text{ cm}$ etching areas of individual die to free the microneedles from the wafer backside. A timed EDP etch reduces the silicon wafer thickness to $120\text{ }\mu\text{m}$. After a DI rinse, the wafer is immersed in 5:1 BHF solution which attacks only the pre-opened, bare Si_2O_2 areas as shown in Fig. 3(d). Immersion in EDP in a timed etch reduces the $120\text{ }\mu\text{m}$ thickness down to $50\text{ }\mu\text{m}$ at the shank end of the microneedle (as seen in Figs. 3(e) and 1). As is evident in Fig. 2(b), no single-crystal silicon is left at the tip region of the microneedle owing to the corner-etching behavior of EDP [18]. A combination of corner etching and etching from the crystal backside also removes the thicker nondoped single-crystal silicon for about $50\text{ }\mu\text{m}$ along the needle underside from the tip end. A shallow plasma etch

by using SF_6 can be used to remove a thin nitride layer and open the contacts. The nitride cover for the flow channel has sufficient thickness so that the flow channels are not damaged by this final etch.

The ability to construct electrodes to the microneedles is important for neural measurements. This can be done by modifying the above process. First, the polysilicon layer can be used as interconnection for electrical passage from the distal to the shank end. Second, Mask #7 in the above process will be modified to open the electrodes on the tip region of the microneedle and the contact pads at the same time. The etching process will remove the nitride layer all the way to polysilicon. Lift-off process is then used to deposit a thin layer of sputtered Ti (500 \AA) and Pt (5000 \AA). Ti layer serves as an adhesion layer and Pt is chosen for its excellent biocompatibility and good compatibility with EDP etching [4]. Finally, the back side of the wafer is patterned with a blank mask as before and the wafer can follow the same EDP etching processes to free the microneedles.

IV. RESULTS AND DISCUSSIONS

Fig. 4 is an optical micrograph showing two needles, 1- and 3-mm-long, together with a human hair to provide a scaling

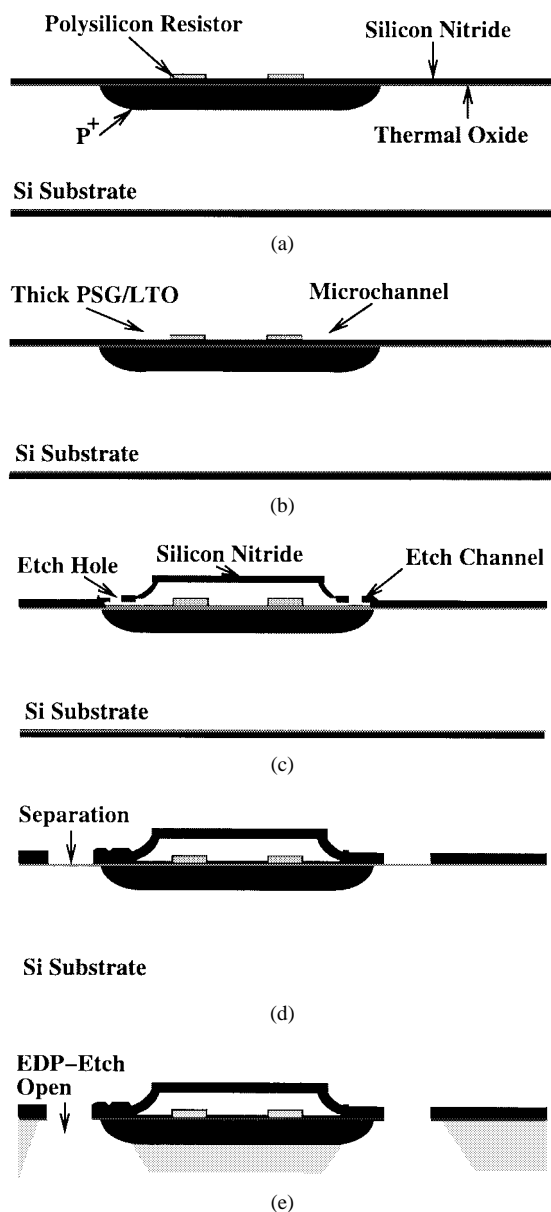


Fig. 3. Process sequences of silicon processed microneedles.

reference. Although the mismatch of thermal coefficient of different layers on the microneedles could cause them to curl [4], this is not observed in the figure. The bubble-pumping resistors and pads can be seen in the shank region, and the stubs from the beams which were broken when the needles were removed from their substrates are clearly visible. The 3-mm-long microneedle tapers from the tip end, where it is 80 μm wide to 140 μm where it joins the shank in order to increase strength. Tapering was not designed for the 1-mm needle, which is uniformly 80 μm wide.

Fig. 5 is a micrograph of the tip region of a microneedle, showing etch holes and the distal fluid port. The tip is formed with an approach angle of 44 degrees on the surface plane. When finished, the microchannel has a width of 50 μm and a height of 9 μm . The distal fluid port is positioned 150 μm up the needle from the tip with a square pattern of 30 μm at each side. Figs. 6 and 7 are two scanning electron

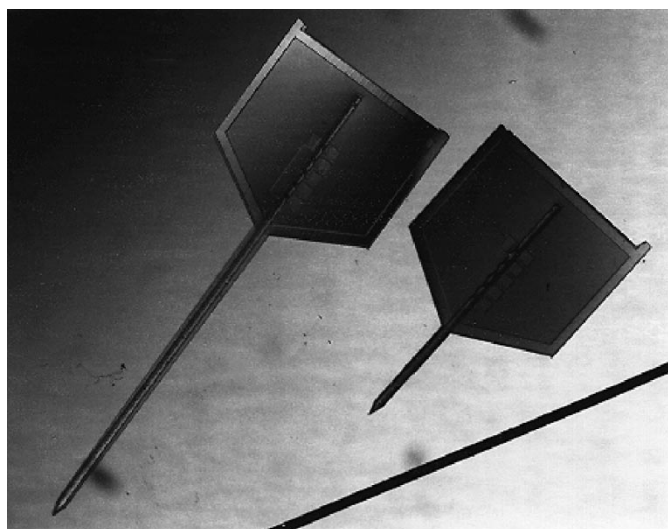


Fig. 4. Two silicon microneedles placed alongside a human hair.

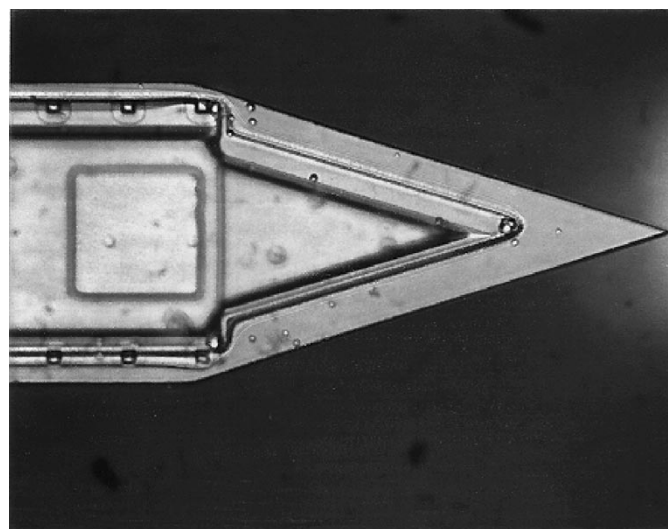


Fig. 5. Top view (optical microscope) showing the tip end of a microneedle.

microscope (SEM) views of the top and side of a microneedle, respectively. Bubbles are seen in Fig. 6, and it is possibly from the thick PSG deposition process. Shown in Fig. 7 are the bottom heavily doped single-crystal silicon layers with a thickness of about 12 μm . Above this boron etch stop region is a thin layer of thermal oxide. It is followed up by a layer of approximately 3 μm of low-stress silicon nitride. The nitride layer also forms the top of the microchannel structure which is about 10 μm in total height.

Fig. 8 is a near “head-on” view of a free-standing microneedle as seen in a scanning electron microscope micrograph. At the far side of the photo, the IC-interface region with irregular shape of single-crystal silicon underneath is dimly seen with about 50 μm remaining. The single-crystal silicon layer underneath the microneedle can be clearly seen in the close-up SEM micrograph in Fig. 9. The damage to the microneedle tip seen in Fig. 9 occurred while preparing the sample for viewing in the SEM. The etch holes, fluid port, and boron stop can also be seen here; in this needle the port

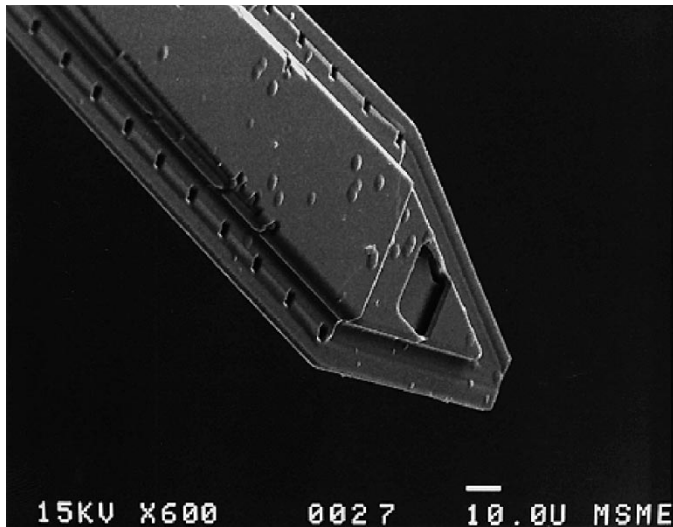


Fig. 6. Top view (SEM) showing the tip end of a microneedle.

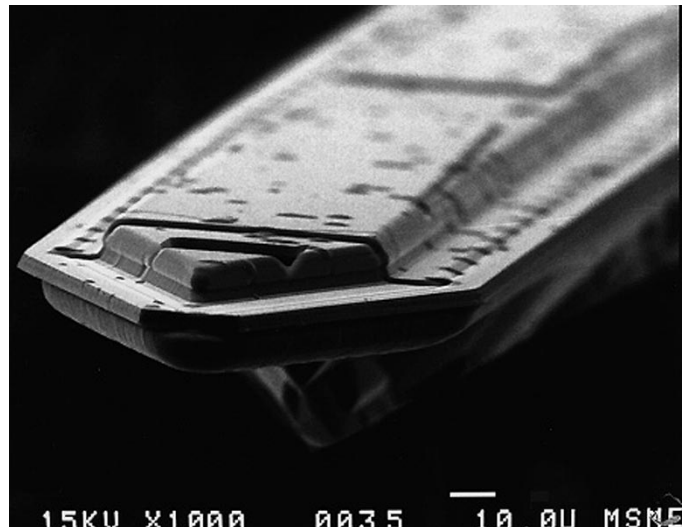


Fig. 9. Close view of Fig. 8 showing the tip of the microneedle with single-crystal silicon underneath at the rear part.

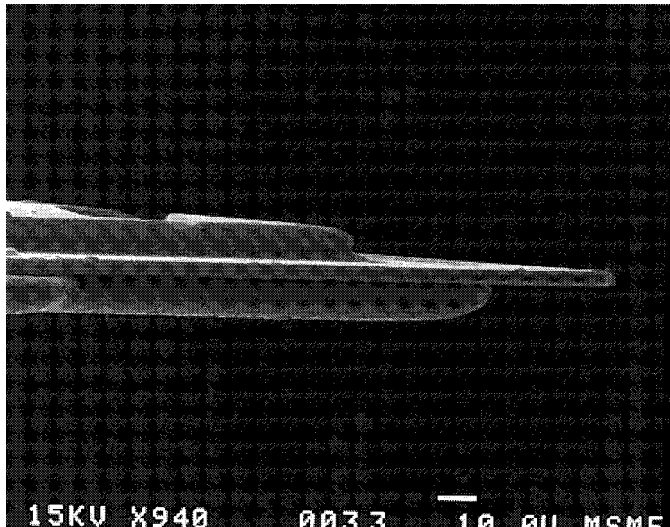


Fig. 7. Side view of the tip end of a microneedle as seen in a SEM.

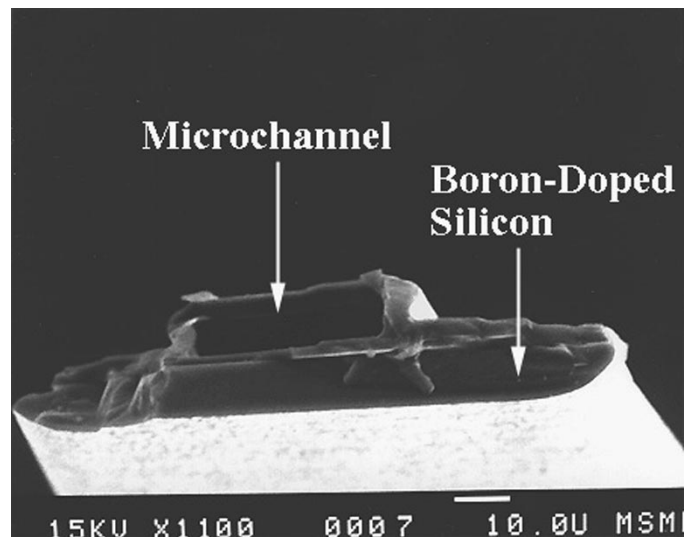


Fig. 10. Cross section (near tip) of the microneedle after cleaving the microneedle.

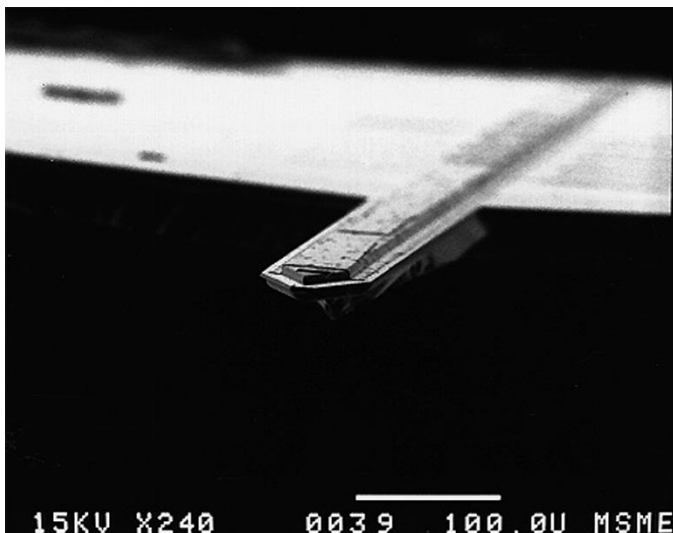


Fig. 8. Near "head-on" view of a free-standing microneedle as seen in an SEM micrograph.

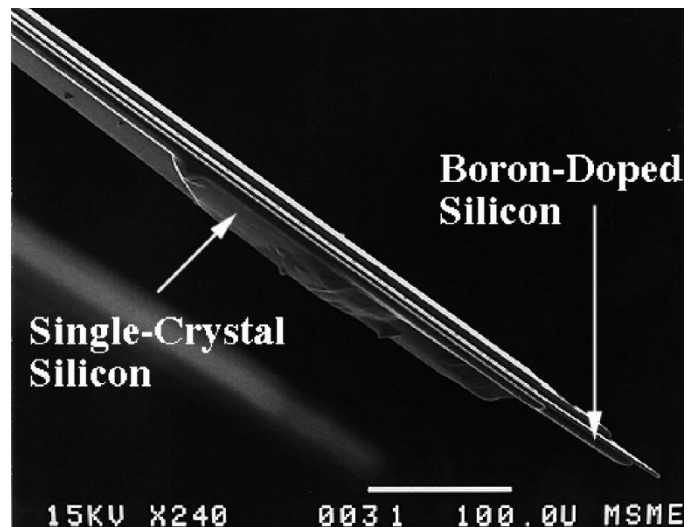


Fig. 11. Side view of a whole microneedle showing silicon left underneath.

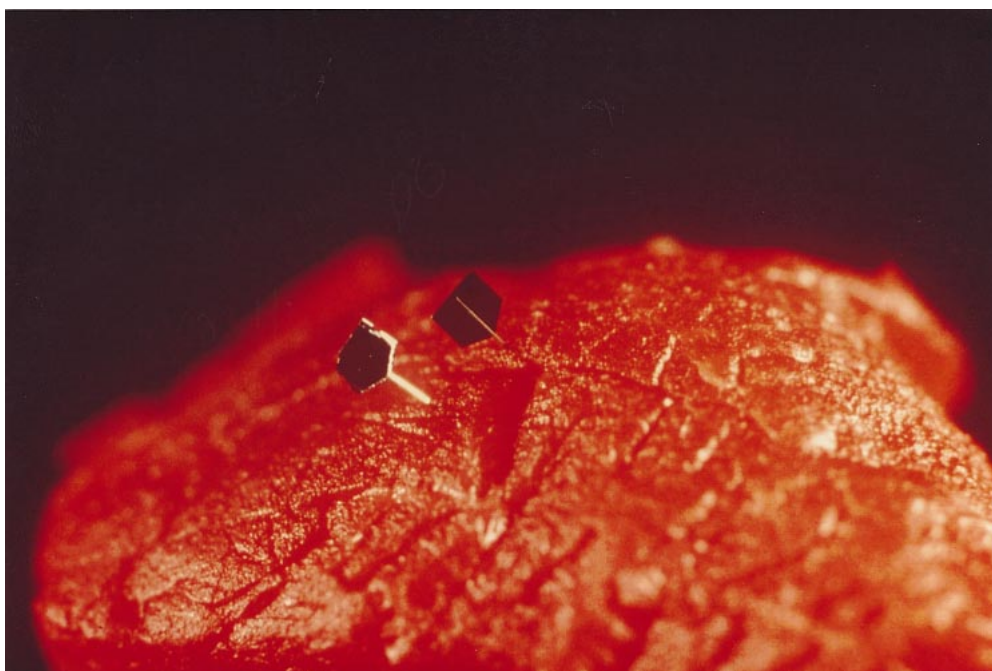


Fig. 12. Two microneedles penetrating porterhouse steak.

is situated on the triangle part of the tip instead of further back as in the needle shown in Fig. 5. Fig. 10 is an SEM cross section of a microneedle which has been cleaved near the tip. The microchannel has a slightly smaller width than the standard ones and its dimensions are $9 \times 30 \mu\text{m}^2$ as seen in the micrograph. This cross section was taken from the front portion of the microneedle and the surface of single crystal silicon with heavily doped boron can be clearly identified.

The fabricated microneedles have a layer of single-crystal silicon left to increase the strength as seen in Fig. 11. However, silicon at the tip region has been etch away due to the corner effect such that the needle may also function well for neural measurement applications. The imperfection of the single crystal silicon underneath the microneedle is the result of uneven corner attack etching in the EDP. Shown in Fig. 12 are two microneedles, respectively 1 and 6 mm-long, stuck into muscle tissue (porterhouse steak¹). Penetration was easily accomplished without any needle breakage or bending. Najafi and Hetke [23] have reported bending in 15- μm -thick silicon probes made by another process when they attempted to penetrate animal tissue. Since the buckling force on the needle depends cubically on its thickness, our microneedles with thickness of 70 μm (microchannel height, boron region plus single crystal region) should be roughly 100 times stronger in buckling resistance.

Fig. 13 is a photograph taken after the completion of the micromachining process. The microneedle is still connected to the substrate via two mechanical beams that are made of heavily boron-doped silicon. These mechanical supports are sufficiently rigid to hold microneedles but can be easily broken in order to separate needles from the substrate. This design feature makes easier transport and packaging than if all needles were fully freed during the final etching process [4]. Fig. 14

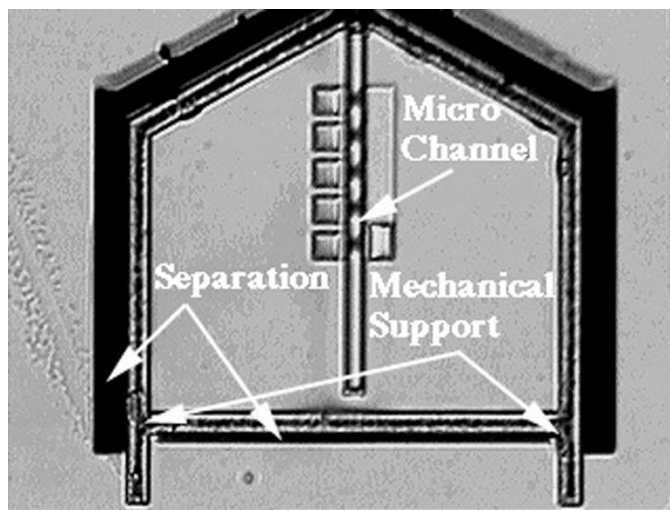


Fig. 13. Close view (optical microscope) showing mechanical supports and the separation area (black color).

shows the back side of a processed wafer. Most microneedles were picked away for experiments with few left in the figure. In this trial run, a conservative design rule is used and only the area that consists of 32 die is etched in EDP. These openings with size of 1 cm \times 1 cm are defined by using a blank mask via a wafer stepper. The truss-structures between individual die are preserved to increase the rigidity of the substrate for easy handling.

V. SUMMARY

Design and fabrication of silicon-processed microneedles by combined surface and bulk micromachining processes have been described. The microneedles have on-board resistive heaters for bubble-pumping elements, two fluid ports for liquid transport, and an IC-interface region that can be used for future on-chip circuitry and microfluidic components. In the single

¹New York Style.

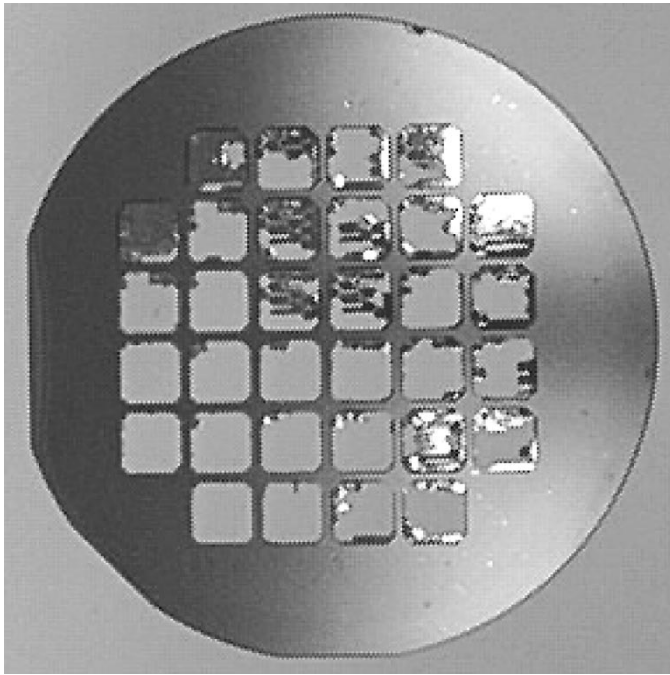


Fig. 14. Back side of the wafer after the completion of the microfabrication process.

run-through of the process described, which avoids the need for backside alignment, a yield of 90% of completed needles was obtained. An advantage of the process is that it provides needles that are surrounded by regions of silicon having full wafer thickness. This feature simplifies postprocessing, handling, and lead attachment which can be accomplished prior to freeing the needle by breaking support beams. The microneedles have been sufficiently robust to penetrate muscle tissue without being damaged. The seven-mask fabrication process is compatible with IC processes.

ACKNOWLEDGMENT

The authors would like to give special thanks to Prof. Muller for his technical and editorial suggestions. They would also like to thank Profs. K. D. Wise and K. Najafi at the University of Michigan for valuable discussions, R. Wilson for taking SEM micrographs, and the staff at the UCB microlab for help and suggestions. The devices were fabricated in the UC Berkeley Microfabrication Laboratory.

REFERENCES

- [1] L. Lin, A. P. Pisano, and R. S. Muller, "Silicon processed microneedles," in *Dig. Transducers'93, Int. Conf. Solid-State Sensors and Actuators*, 1993, pp. 237–240.
- [2] J. Chen and K. D. Wise, "A multichannel neural probe for selective chemical delivery at the cellular level," in *Tech. Dig. IEEE Solid-State Sensor and Actuator Workshop*, June 1994, pp. 256–259.
- [3] N. H. Talbot and A. P. Pisano, "Polymolding: Two wafer polysilicon micromolding of closed-flow passages for microneedles and microfluidic devices," in *Tech. Dig. Solid-State Sensor and Actuator Workshop*, June 1998, pp. 265–268.
- [4] K. Najafi, K. D. Wise, and T. Mochizuki, "A high-yield IC-compatible multichannel recording array," *IEEE Trans. Electron Devices*, vol. ED-32, pp. 1206–1211, 1985.
- [5] L. Lin and A. P. Pisano, "IC-processed microneedles," U.S. Patent 5 591 139, 1997.
- [6] ———, "Thermal bubble powered microactuators," *Microsyst. Technol.*, vol. 1, pp. 51–58, 1994.

- [7] L. Lin, "Microscale thermal bubble formation: Thermophysical phenomena and applications," *Microscale Thermophys. Eng.*, vol. 2, pp. 71–85, 1998.
- [8] L. Lin, K. S. Udell, and A. P. Pisano, "Liquid-vapor phase transition and bubble formation in micro structures," *Thermal Sci., Eng.*, vol. 2, pp. 52–59, 1994.
- [9] T. K. Jun and C.-J. Kim, "Microscale pumping with traversing bubbles in microchannels," *Solid-State Sensors and Actuators Workshop*, 1996, pp. 144–147.
- [10] R. M. Moroney, R. M. White, and R. T. Howe, "Microtransport induced by ultrasonic lamb waves," *Appl. Phys. Lett.*, vol. 59, pp. 774–776, 1991.
- [11] M. Esashi, "Integrated micro flow control systems," *Sensors and Actuators*, vol. 21A, pp. 161–167, 1990.
- [12] S. Shoji, S. Nakagawa, and M. Esashi, "Micropump and sample-injector for integrated chemical analyzing systems," *Sensors and Actuators*, vol. 21A, pp. 189–192, 1990.
- [13] H. T. G. Van Lintel, F. C. M. Van Deptol, and S. Bouwstra, "A piezoelectric micropump based on micromachining of silicon," *Sensors and Actuators*, vol. 15, pp. 153–167, 1988.
- [14] S. F. Bart, L. S. Tavrow, M. Mehregany, and J. H. Lang, "Microfabricated electrohydrodynamic pumps," *Sensors and Actuators A-Physical*, vol. 21, pp. 193–197, 1990.
- [15] A. Richter, A. Plettner, K. A. Hofmann, and H. Sandmaier, "A micromachined electrohydrodynamic (edh) pump," *Sensors and Actuators*, vol. 29A, pp. 159–168, 1991.
- [16] C. H. Mastrangelo, J. H. Yeh, and R. S. Muller, "Electrical and optical characteristics of vacuum-sealed polysilicon microlamps," *IEEE Transactions on Electron Devices*, vol. ED-39, pp. 1363–1375, 1992.
- [17] L. Lin, K. M. McNair, R. T. Howe, and A. P. Pisano, "Vacuum encapsulated lateral microresonators," in *Dig. Transducers'93, Int. Conf. Solid-State Sensors and Actuators*, 1993, pp. 270–273.
- [18] B. Bassous, "Fabrication of novel three-dimensional microstructures by the anisotropic etching of (100) and (110) silicon," *IEEE Trans. Electron Devices*, vol. ED-25, pp. 1178–1185, 1978.
- [19] C. J. Kim, A. P. Pisano, and R. S. Muller, "Silicon-processed overhanging microgripper," *J. Microelectromech. Syst.*, vol. 1, pp. 31–36, 1992.
- [20] K. Takahashi and T. Matsuo, "Integration of multi-microelectrode and interface circuits by silicon planar and three-dimensional fabrication technology," *Sensors and Actuators*, vol. 5, pp. 89–99, 1984.
- [21] L. I. Maissel and R. Chang, Eds., *Handbook of Thin Film Technology*. New York: McGraw-Hill.
- [22] L. Lin, K. S. Udell, and A. P. Pisano, "Vapor bubble formation on a micro heater in confined and unconfined micro channels," in *Proc. ASME 29th Nat. Heat Transfer Conf.*, vol. HTD, no. 253, pp. 85–94, 1993.
- [23] K. Najafi and J. F. Hetke, "Strength characterization of silicon microprobes in neurophysiological tissues," *IEEE Trans. Biomed. Eng.*, vol. 37, pp. 474–481, 1990.



Liwei Lin received the B.S. degree in power mechanical engineering from National Tsing Hua University, Taiwan, Republic of China, in 1986 and the M.S. and Ph.D. degrees in mechanical engineering from the University of California, Berkeley, in 1991 and 1993, respectively.

He joined BEI Electronics Inc. USA from 1993 to 1994 in research and development of microsensors. From 1994 to 1996, he was an Associate Professor in the Institute of Applied Mechanics, National Taiwan University, Taiwan. Since 1996, he has been an Assistant Professor at the Mechanical Engineering and Applied Mechanics Department at University of Michigan. He joined the Berkeley Sensor & Actuator Center, an NSF/Industry/University research cooperative center as a research assistant during his graduate study. His research interests are in microelectromechanical systems, including design, modeling, and fabrication of microstructures, microsensors, and microactuators.

Dr. Lin is the recipient of the 1998 NSF CAREER Award for research in MEMS packaging. He is currently serving as the Chairman of the Microelectromechanical Systems (MEMS) Panel of the ASME Dynamics Systems and Control Division and is leading the effort in establishing a new MEMS Division in ASME. He holds five U.S. patents in the area of MEMS.

Albert P. Pisano, for a photograph and biography, see this issue, p. 33.